Mid-infrared polarization beam splitter based on square/circular hybrid air holes with wide bandwidth and ultrashort length

Guang-ming Zheng

School of Electronics Engineering of Xi'an University of Posts and Telecommunications,
Xi'an, 710121, China; 2023871894@qq.com

A novel mid-infrared polarization beam splitter (PBS) based on GaS is proposed. The high birefringence is achieved by using the cladding structure of alternating arrangement of square and circular air holes as well as introducing double elliptical air holes. The finite element method (FEM) is utilized to investigate the mode coupling characteristics in the proposed PBS. The results show that the highest extinction ratio of 115 dB and shortest length of only 40 μm can be realized at a wavelength of 4 μm. A wide bandwidth of 200 nm ranging from 3.9 to 4.1 μm is obtained.

Keywords: polarization beam splitter, mid-infrared, photonic crystal fiber, bandwidth, square and circular air hole.

1. Introduction

The light polarization management is a crucial issue in optical fiber communication, sensing and other optical systems because many linear and nonlinear optical effects are polarization-dependent [1]. The most prominent feature of light polarization is that it is very vulnerable to environmental factor variations including temperature fluctuation, mechanical vibration, and tension change. Moreover, many optical devices are greatly polarization-dependent including optic fiber gyroscope, all-optical wavelength converter, optical time-division demultiplexer, and so on [2–4]. Therefore, the random variation of the light polarization in the optical transmission or measurement system will give rise to various adverse optical effects, and eventually lead to the performance degradation of the optical system. In order to realize polarization independent operation of an optical system, various polarization manipulation devices or polarization diversity scheme have been put forward to construct a polarization transparent system [5, 6]. Polarization beam splitter (PBS) is one of the most basic polarization handling devices, which can separate input light with random polarization states into two orthogonal polarization components along different pathways propagation [7]. It plays a very crucial role in coherent optical communication [8], optical-fiber sensing [9], photopo-

larimeters [10], quantum optics information system [11] and passive mode-locked fiber laser [12–15].

As early as the 1990s, several PBSs have been fabricated by using conventional optical fiber, but their outstanding disadvantage is that the length of PBSs is too big to meet the requirements of integration and miniaturization of photonic system [16, 17]. Recently, quite a few PBSs based on silicon-on-insulator (SOI), indium phosphide (InP) and lithium-niobate-on-insulator (LNOI) platforms are reported [18–20]. Some new structures with high performance have been proposed and demonstrated including symmetrical/asymmetric directional couplers [21, 22], partially etched multimode interference couplers [23], Mach–Zehnder interferometers (MZIs) [24], tapered waveguides [25], coupled plasmonic waveguide arrays [26] and sub-wavelength grating (SWG) [27]. Nevertheless, most of them have relatively complex structures. Moreover, the rigorous fabrication tolerance ultimately hinders their engineering application in large scale photonic integration circuits (PICs).

More recently, PBSs based on photonic crystal fiber (PCF) have attracted a lot of attention due to the advantages of broad bandwidth and compatible with current optical fiber communication systems. Moreover, because of the flexible air hole structure and extraordinary properties of PCF [28], PBSs based on PCF are more efficient and compact, which cannot be realized by conventional optical fibers. Several PCF-based PBSs with short length have been reported. For example, in 2005, a dual-core PCF based PBS was reported by uniformly distributed elliptically-shaped air holes in the cladding of a PCF [29]. The bandwidth of 5.1 nm at 1.55 µm and coupling length of 15.4 mm was obtained. In 2013, Lu proposed an 84.7-mm long PBS with 300 nm-bandwidth based on a modified three-core PCF [30]. In 2015, JIANG obtained a 4.036-mm long PBS with 430 nm-bandwidth at 1.55 µm based on a square-lattice dual-core PCF [31]. In 2018, WANG realized a 78-µm long PBS with 44 nm-bandwidth at 1.55 µm based on a liquid-filled dual-core PCF [32]. In 2019, ZHAO proposed a 6.75-cm long ultra-broadband PBS with 310 nm bandwidth based on dual hollow-core anti-resonant PCF [33]. However, we can see that all previously reported PBSs mainly work in the near infrared (near-IR) waveband. In recent years, the mid-infrared (mid-IR) waveband (located between near-IR and far-IR wavelengths) has attracted great interest because of its broad atmospheric window and unique gas molecular absorption peaks in this region [34]. The mid-IR band has been widely used in optical communication, biotechnology, spectroscopy, food safety, environmental monitoring, and other fields [35]. But up to now, PBS working in mid-IR region is rarely reported. Until recently, two kinds of mid-IR PBSs based on metasurface-assisted silicon nitride Y-junction and surface plasmon resonance-enhanced silicon dual-core PCF are proposed, respectively [36, 37].

Nevertheless, they are not practical for engineering application in terms of cost, bandwidth and transmission loss. It is challenging to design mid-IR PBS with large bandwidth and low loss.

In this paper, a novel mid-IR PBS with wide bandwidth and ultrashort length based on GaS dual core PCF is proposed. By introducing a pair of elliptical air holes into fiber

core and using square and circular hybrid holes cladding, efficient polarization splitting with a bandwidth of 300 nm in the mid-IR region is obtained with device length of only 40 μm. The maximum polarization extinction ratio (ER) of 115 dB is realized at 4 μm for the proposed PBS. The proposed PCF based PBS is fully compatible with popular optical fiber system and will play an important role in mid-IR photonics.

2. Structure of the GaS-based PCF-PBS

Figure 1 is the schematic cross-section of the proposed ultra-short dual-core GaS-based PCF-PBS. The white regions denote air holes. The blue regions are substrate material. In view of its wide transparent window and excellent mechanical durability in mid-IR region, GaS is used as fiber substrate material. The proposed PBS is based on a triangular lattice structure which is composed of circular and square air holes. The whole air hole array is rectangular. Two circular air holes and two square air holes are missing in the center of the PBS to form a fiber core, and two elliptical holes arranged along the vertical direction are inserted to divide the fiber core into left and right dual core structures. The cladding air holes are alternately arranged by circular air holes and square air holes. The radius of circular hole in cladding is $d_1 = 0.4$ μm, and the side length of square air hole is $d_2 = 1$ μm. The transverse distance between the center of the circular air hole and the center of the square air hole is e_1, and the longitudinal distance is e_2. The long half axis of the central elliptical air hole is $a = 0.6$ μm, and the short half axis is $b = 0.22$ μm. In this structure, on the one hand, the high birefringence
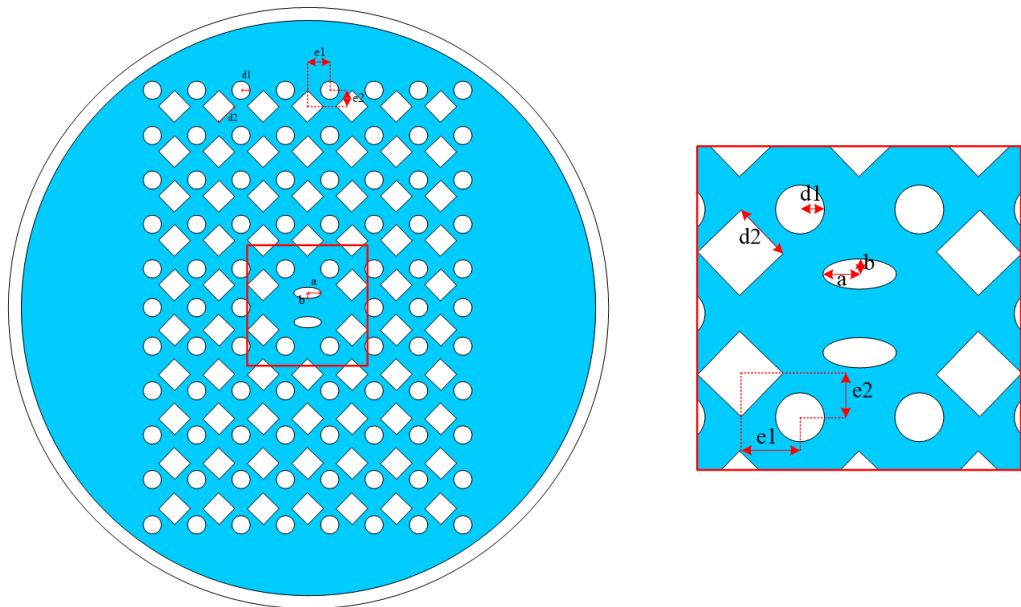

Fig. 1. Schematic cross-section of the proposed PBS with square and circular air holes in the PCF cladding.

is increased by using the alternate cladding structure of square air hole and circular air hole; on the other hand, the structure symmetry of the PCF is destroyed by introducing the elliptical air holes in the core, so that the birefringence is increased further, which is convenient for the complete separation of x and y polarized light. To optimize the PBS geometric structure and evaluate its performance, the finite element method (FEM) combined with rectangular perfect matching layer (PML) absorption boundary is used to analyse the mode coupling properties. In the numerical calculation, the mesh resolution is $\lambda/12$. The refractive index of the air hole is 1, and the refractive index of GaS is obtained by using the Sellmeier equation [38]

$$n(\lambda) = \sqrt{A + \frac{B\lambda^2}{\lambda^2 - C} + \frac{D\lambda^2}{\lambda^2 - E}} \tag{1}$$

Here $A = 7.12996$, $B = 0.26073$, $C = 0.04627$, $D = 127.335$, and $E = 258.431$.

When light with arbitrary polarization injected into PCF, two orthogonal polarization components are coupled with each other in two cores. The coupling length of the dual core PCF in x- and y-polarization direction can be obtained through the following equation [31]

$$L_i = \frac{\lambda}{2\left|n_e^i - n_o^i\right|}, \quad i = x, y \tag{2}$$

Here λ is a wavelength of incident light in vacuum, n is effective refractive index, the superscript i refers to x- and y-direction polarization, the subscripts o and e describe odd mode and even mode. Due to the asymmetry of fiber structure, the even and odd modes in x- and y-directions have different effective refractive indexes. When the transmission length is $L = mL_x = nL_y$, the two orthogonal polarization components will be separated completely. For clarification, a crucial parameter of coupling length ratio (CLR) is defined by the following equation [31]

$$\text{CLR} = \frac{L_y}{L_x} = \frac{m}{n} \tag{3}$$

The shortest PBS length can be obtained when CLR is 2 ($L_x < L_y$) or 1/2 ($L_x > L_y$). When the incident light launched into port A of proposed PBS, it can transform energy between core A and core B periodically along transmission length. The output power at core A can be obtained by [31]

$$P_{i\text{-out}} = P_{\text{in}}\cos^2\left(\frac{\pi L}{2L_i}\right) \tag{4}$$

Here P_{in} are the input optical power. L_i denotes coupling length in x- and y-direction, respectively. The polarization ER is defined as the ratio of the optical power of one spe-

cific polarization to the optical power of another vertical polarization in the same fiber core at the PBS output end. It can be calculated through the following equation [31]:

$$ER = 10 \log_{10} \frac{P^{y}_{out}}{P^{x}_{out}} \tag{5}$$

3. Structure optimization and discussion

From the viewpoint of practical applications such as optical communication, toxic gases monitoring and so on, PBS with large bandwidth and short device length is highly desirable. According to waveguide optics and coupling mode theory, the guided wave properties of PCF are dependent on the air hole size, shape, and lattice constants. These geometrical parameters will ultimately determine the mode properties of PCF. Then, by suitable designing the PCF cross-section through optimizing structural parameters, the efficient mode field coupling can be realized between even and odd modes in x- and y-polarized direction, respectively. Therefore, in the following section, to obtain a PBS with broad bandwidth and ultrashort length, we will investigate the influence of PBS geometric parameters (including a, b, d_1, d_2, e_1, and e_2) on the mode coupling properties by using FEM numerical method. The dependences of CL (including L_x and L_y), CLR and PBS structural parameters are analyzed carefully.

Firstly, we investigate the dependence of L_x, L_y and CLR on the structure parameters a. In this simulation, $d_1 = 1$ μm, $d_2 = 0.4$ μm, $e_1 = 2.02$ μm, $e_2 = 1.5$ μm, $b = 0.22$ μm. a is increased from 0.56 to 0.64 μm. The results are shown in Fig. 2**a**. Obviously, with the increase of a, the coupling length L_x is almost unchanged, L_y increases slowly, and CLR increases significantly. But for all a, L_y increases faster than L_x. It can be explained that with the increase of a, the asymmetry of PBS core increases, which increases the birefringence effect and compresses the core mode field. On the other hand, we can find that CLR increases with the increase of a in the wavelength range of 0.56 to 0.64 μm. This is because when a increases, the birefringence in x-polarization direction is stronger than that in y-polarization direction. It can be found that when a is 0.6 μm, the CLR is close to 2. Therefore, $a = 0.6$ μm is selected as the best value of the long axis radius.

Secondly, we investigate the dependence of L_x, L_y and CLR on the structure parameters b. In this simulation, $d_1 = 1$ μm, $d_2 = 0.4$ μm, $e_1 = 2.02$ μm, $e_2 = 1.5$ μm, $a = 0.6$ m. b is increased from 0.18 to 0.26 μm. The results are shown in Fig. 2**b**. It can be observed from Fig. 2**b** that when the parameter b increases, L_x and L_y increase obviously. At the same time, CLR decreases slightly with the increase of b. It can be explained that when b increases, the asymmetry of the two cores of the PBS increases, which makes the birefringence effect increase. Moreover, the increment of birefringence is different in x and y directions.

Third, the dependence of L_x, L_y and CLR on the structure parameters d_1 and d_2 are investigated. In this simulation, d_1 increases from 0.96 to 1.04 μm while other param-

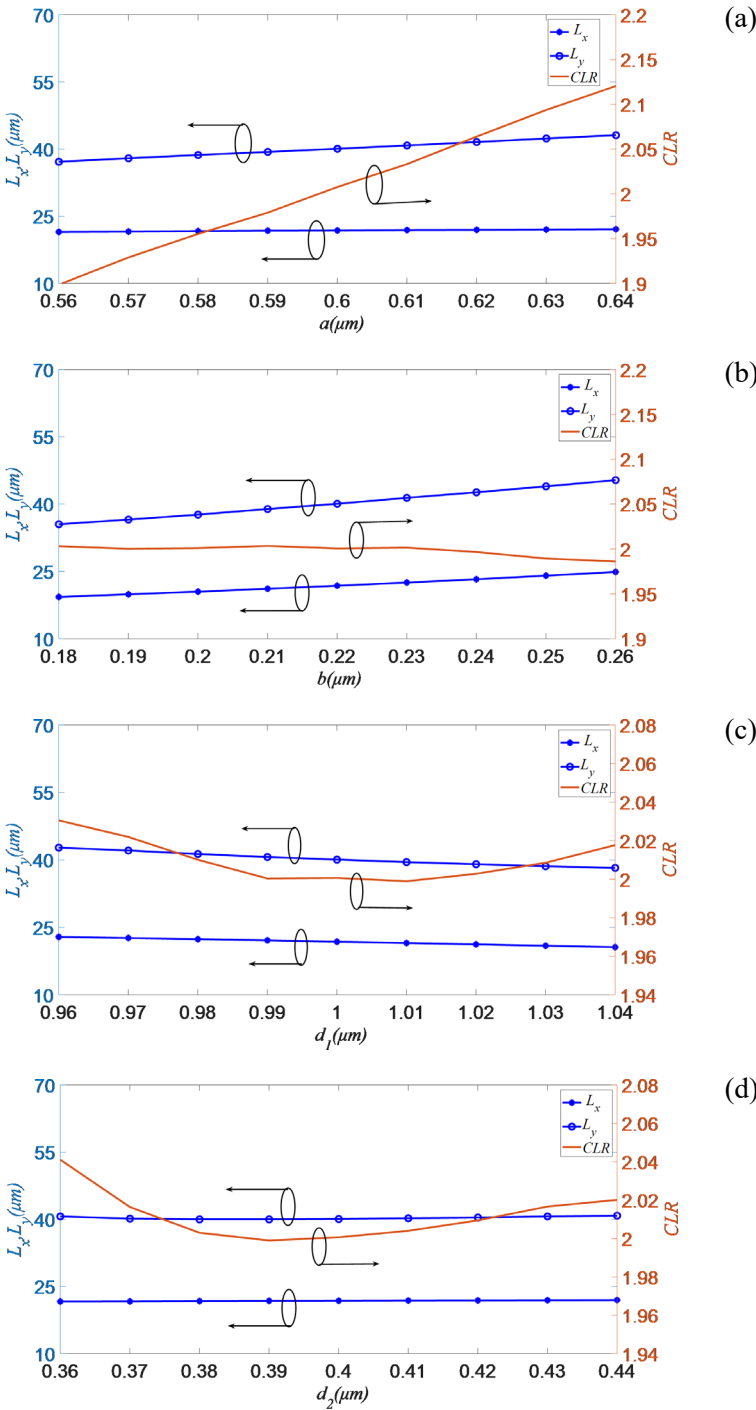Fig. 2. The L_x, L_y and CLR as a function of wavelength for proposed PBS parameters of (**a**) a, (**b**) b, (**c**) d_1, (**d**) d_2, (**e**) e_1, and (**f**) e_2.
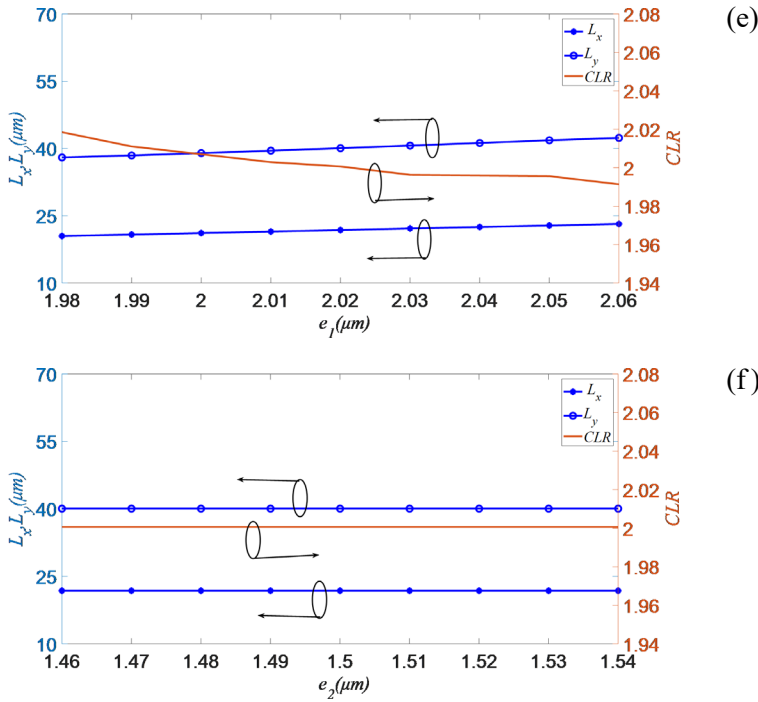
Fig. 2. Continued.

eters are fixed. The results are given in Fig. 2**c**. Obviously, with the increase of d_1, the coupling lengths L_x, and L_y decrease. However, the evolution trend of CLR is decreasing first and then increasing. When d_1 increases from 0.96 to 1.01 μm, the enhancement of birefringence in x-direction is smaller than that in y-direction, so CLR decreases with the increase of d_1. When d_1 increases from 1.01 to 1.04 μm, the enhancement of birefringence in x-direction is larger than that in y-direction, so CLR increases. Figure 2**d** describes the dependence of L_x, L_y and CLR on the structure parameters d_2. Clearly, the evolution trend of the curves is like that of Fig. 2**c**. L_x and L_y increase with the increase of d_2, but CLR first decreases and then increases. It can be found that when d_1 and d_2 are 1 and 0.4 μm, respectively, the CLR is close to 2. So d_1 = 1 μm and d_2 = 0.4 μm are selected as the optimal values of the circular hole radius and square hole side length.

Finally, the dependences of L_x, L_y and CLR on the structure parameters e_1 and e_2 are investigated. Figure 2**e** describes the dependence of L_x, L_y and CLR on the structure parameters e_1. In this simulation, e_1 increases from 1.98 to 2.06 μm while other parameters are fixed. Obviously, with the increase of e_1, the coupling lengths L_x, and L_y increase slowly while CLR decreases. It is due to the fact that birefringence variation in x-direction is smaller than that in y-direction. Figure 2**f** describes the dependence of L_x, L_y and CLR on the structure parameters e_2. In this simulation, e_2 increases from 1.46 to 1.54 μm while other parameters are fixed. Obviously, the L_x, L_y and CLR are

almost invariable with the increase of e_2. The reason is that when e_2 increases, it has little impact on the asymmetry between the two cores of the PBS, and the birefringence effect is not obvious. It can be found that when e_1 and e_2 are 1 and 0.4 μm, respectively, the CLR is close to 2. So $e_1 = 1$ μm and $e_2 = 0.4$ μm are selected as the optimal values of the transverse distance and longitudinal distance. Based on the above analysis, a set of optimized parameters of $a = 0.6$ μm, $b = 0.22$ μm, $d_1 = 1$ μm, $d_2 = 0.4$ μm, $e_1 = 2.02$ μm and $e_2 = 1.5$ μm is selected as the optimal PBS structure parameters.

For the optimized PBS, the relationship between effective refractive indices and wavelength is investigated. The results are shown in Fig. 3. Obviously, the effective
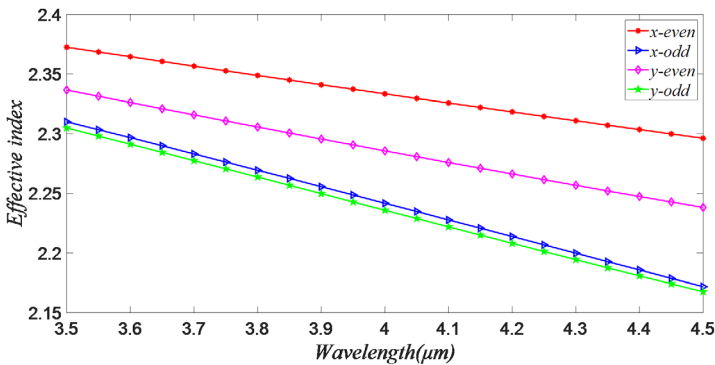

Fig. 3. The effective refractive indexes as a function of wavelength for four super-modes.
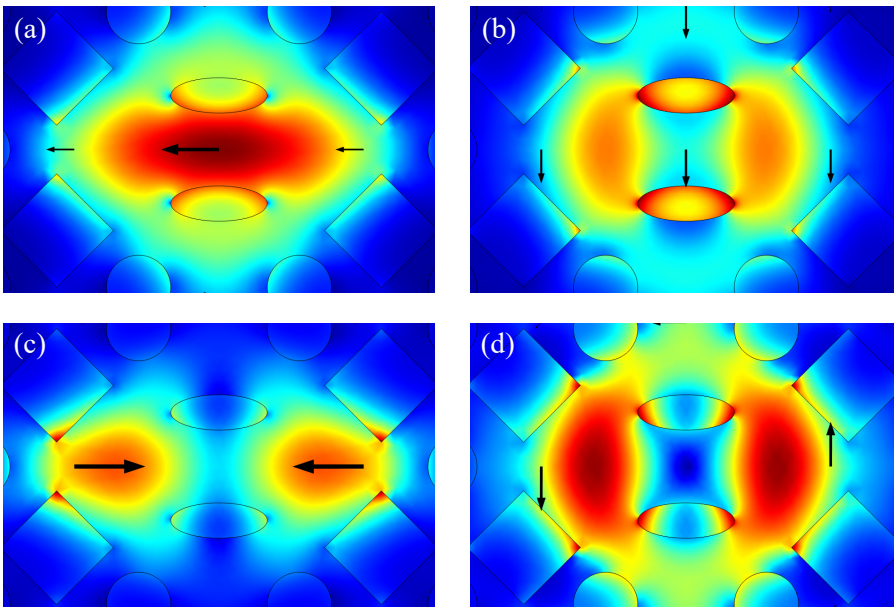

Fig. 4. Distributions of the four supermodes in the proposed GaS-based PCF-PBS: (**a**) the *x*-polarized even mode, (**b**) the *y*-polarized even mode, (**c**) the *x*-polarized odd mode, and (**d**) the *y*-polarized odd mode.

refractive indices of the four super-modes decrease with the increase of wavelength. Nevertheless, due to the asymmetry of the cross-section structure of optimized PCF-PBS, the effective refractive index of the *x*-polarization mode is slightly higher than that of the *y*-polarization mode. In addition, Fig. 4 illustrates the electrical field distributions of two symmetric modes and two asymmetry modes for proposed GaS-based PCF-PBS at a wavelength of 4 μm. The arrows with same direction denote the even mode, including *x*-polarization even mode (see Fig. 4**a**) and *y*-polarization even mode (see Fig. 4**b**). In contrast, the arrows with opposite direction denote odd mode, including *x*-polarization odd mode (see Fig. 4**c**) and *y*-polarization odd mode (see Fig. 4**d**). It can be seen clearly that the light is well confined in the core for all the four super-modes.

Moreover, the variation of CL with wavelength for the proposed PCF-PBS is described in Fig. 5. Obviously, the two CLs decrease with the increase of wavelength. The reason is that with the increase of the wavelength, the mode field gradually expands to the cladding, and the increase of the mode field makes the core coupling effect strengthen, resulting in the decrease of the fiber coupling length. The CL of *y*-direction is larger than that of the *x*-direction from 3.5 to 4.5 μm. For example, the CL of *y*-polarization (L_y) decreases from 64 to 28 μm, while the CL of *x*-polarization (L_x) decreases from 32 to 15 μm. In addition, the difference of L_x and L_y decreases gradually with the increase of wavelength. This can be fully explained by the fact that the effective refractive index difference in *x*-direction is greater than that in *y*-direction in Fig. 5.
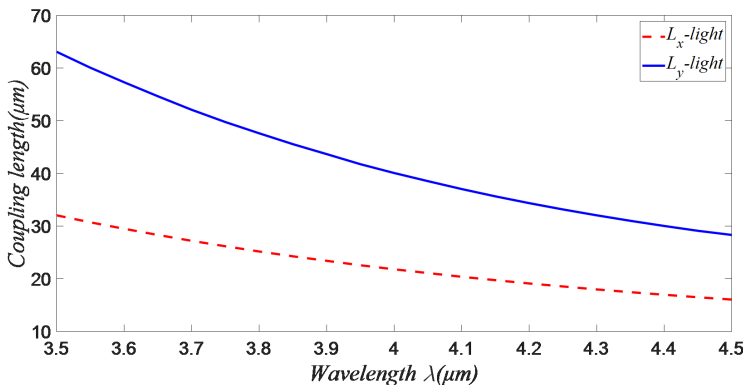

Fig. 5. Coupling length as a function of wavelength.

In order to explain the energy coupling process of different polarization components of incident light in the proposed PBS, according to the coupled mode equation, we plot the evolution curves of *x*- and *y*-polarized light powers along the propagation distance. In the calculation, it is assumed that the incident light is in mid-IR region with a wavelength of 4 μm, which enters the one core of the proposed PBS. Figure 6 describes the calculated normalized output powers of *x*- and *y*-polarization along the propagation distance. Clearly, in the process of transmission, the optical powers of *x*- and *y*-polarization components change periodically along the propagation distance.
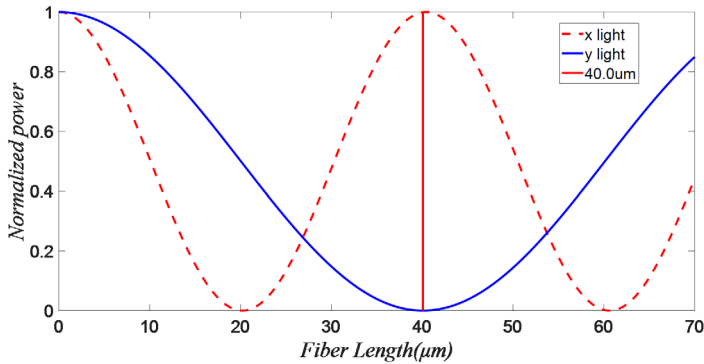
Fig. 6. Normalized output powers of *x*- and *y*-polarization lights.

The out power of *x*-polarization is largest while the *y*-polarization power is close to zero at a propagation distance of 40 μm. Therefore, the two polarization modes are completely separated at the splitter length of 40 μm.

    In generally, when the ER of PBS is better than –20 dB, the incident light for the *x*- and *y*-polarizations are regarded to be separated. Therefore, the ER determines the available bandwidth of a PBS. For our designed dual-core GaS-based PBS, Fig. 7**a** shows the ER as a function of the wavelength when the device length is 40 μm. Figure 7**b** is the 3D view to illustrate the dependence of the ER with wavelength and transmission length. It can be found that the ER is higher than 20 dB in the wavelength range from 3.9 to 4.1 μm, so the corresponding bandwidth is as wide as 200 nm. In particular, the ER is even as high as 117 dB at a wavelength of 4 μm. These results reveal that the proposed PBS can obtain an ultrabroad bandwidth of 200 nm in mid-IR region with ultrashort length of only 40 μm.

    Finally, we compare the performance of the proposed PBS in this work with that reported in previous literatures, and the results are shown in the Table. We focus on two important parameters of PBS including device length and bandwidth. As shown
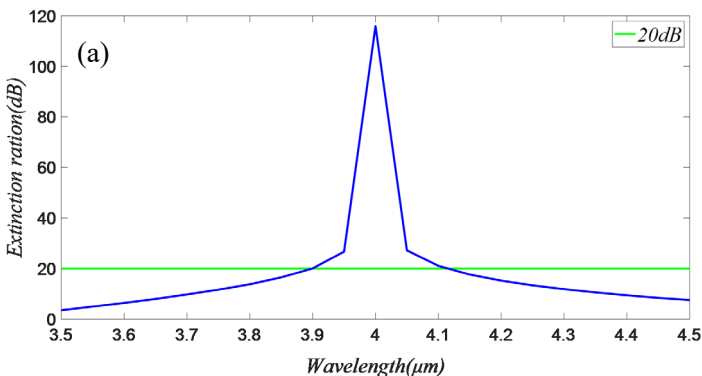

Fig. 7. (**a**) The ER of proposed PBS as a function of wavelength, and (**b**) 3D view of ER *versus* wavelength and propagation distance.
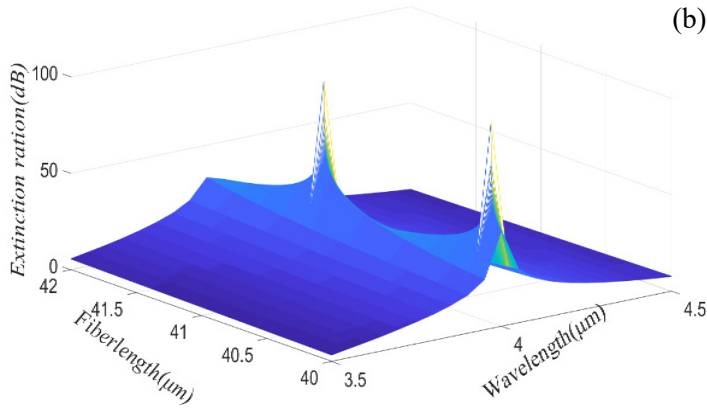
(b)

Fig. 7. Continued.

in the Table, the device lengths of other PBS are all longer than 100 μm, while the device length of our proposed PBS is only 40 μm, which is the shortest compared with other PBS mentioned in the Table. This characteristics make our proposed PBS has great potential for using in photonic integrated system.

T a b l e. The performance comparison of proposed PBS with previous results

References	Device length [mm]	Bandwidth [nm]
2005 Florous *et al*. [29]	15.4	5.1
2013 Lu *et al*. [30]	84.7	300
2013 Sun *et al*. [39]	63	146
2014 Jiang *et al*. [40]	0.1191	249
2014 Chen *et al*. [41]	0.175	250
2015 Jiang *et al*. [31]	4.036	430
2016 Zhao *et al*. [42]	52.8	320
2018 Wang *et al*. [32]	78	44
2019 Zhao *et al*. [33]	67.5	310
This work	0.04 (shortest)	200

4. Conclusion

A novel GaS-based mid-IR PBS with ultrashort length and wide bandwidth based on square and circular hybrid air holes dual core PCF is proposed. The two cores are formed by introducing dual elliptical air holes along vertical direction into the fiber core. The properties of proposed PBS are analyzed by using the full-vector FEM. The results indicate that for the optimized PBS structure, an ultrashort length of only 40 μm and a wide bandwidth of 200 nm are obtained in the mid-IR region. The highest ER up to 115 dB is achieved at a wavelength of 4 μm. The designed PBS obtains perfect combination of ultrashort length, large bandwidth, and high ER in the mid-IR region.

It has great potential for applications in mid-IR fiber laser, optical communication, spectroscopy analysis, and biomedical technology.

Conflicts of interest

The authors declare no conflicts of interest.

References

[1] WANG D., MENYUK C.R., *Polarization evolution due to the Kerr nonlinearity and chromatic dispersion*, Journal of Lightwave Technology **17**(12), 1999, pp. 2520–2529.

[2] CHAMOUN J.N., DIGONNET M.J.F., *Noise and bias error due to polarization coupling in a fiber optic gyroscope*, Journal of Lightwave Technology **33**(13), 2015, pp. 2839–2847.

[3] KRZCZANOWICZ L., CONNELLY M.J., *40 Gb/s NRZ-DQPSK data all-optical wavelength conversion using Four Wave Mixing in a bulk SOA*, Photonics Technology Letters **25**(24), 2013, pp. 2439–2441.

[4] HEDEKVIST P.O., KARLSSON M., ANDREKSON P.A., *Fiber four-wave mixing demultiplexing with inherent parametric amplification*, Journal of Lightwave Technology **15**(11), 1997, pp. 2051–2058.

[5] GALTAROSSA A., PALMIERI L., PIZZINAT A., SCHENATO L., *Polarization mode dispersion management using unidirectionally spun fibers*, Journal of Lightwave Technology **24**(11), 2006, pp. 3976–3981.

[6] FUKUDA H., YAMADA K., TSUCHIZAWA T., WATANABE T., *Silicon photonic circuit with polarization diversity*, Optics Express **16**(7), 2008, pp. 4872–4880.

[7] FAN Z., YUN H., YUN W., *Compact broadband polarization beam splitter using a symmetric directional coupler with sinusoidal bends*, Optics Letters **42**(2), 2017, pp. 235–238.

[8] PÉREZ-GALACHO D., RUIYONG ZHANG, ORTEGA-MOÑUX A., *Integrated polarization beam splitter for 100/400 GE polarization multiplexed coherent optical communications*, Journal of Lightwave Technology **32**(3), 2014, pp. 361–368.

[9] KHAN A., RAZA F., AHMED I., *Optical temperature sensor and switch controlled by competition between phonon and polarization dressing in Pr^{3+}: YSO*, OSA Continuum **3**(2), 2019, pp. 786–796.

[10] AZZAM R.M.A., DE A., *Optimal beam splitters for the division-of-amplitude photopolarimeter*, J. Opt. Soc. Am. A **20**(5), 2003, pp. 955–958.

[11] CRESPI A., RAMPONI R., OSELLAME R., *Integrated photonic quantum gates for polarization qubits*, Nature Communications **2**(1), 2011, p. 566.

[12] SEDDON A.B., TANG Z., FURNISS D., SUJECKI S., BENSON T.M., *Progress in rare-earth-doped mid-infrared fiber lasers*, Optics Express, **18**(25), 2010, pp. 26704–26719.

[13] ZHANQIANG HUI, MENGJIA QU, XIAOHUI LI, *SnS nanosheets for harmonic pulses generation in near infrared region*, Nanotechnology **31**(48), 2020, article 485706.

[14] AYDIN Y.O., FORTIN V., MAES F., *et al.*, *Diode-pumped mid-infrared fiber laser with 50% slope efficiency*, Optica **4**(2), 2017, pp. 235–238

[15] ZHANQIANG HUI, WENXIONG XU, XIAOHUI LI, *Cu_2S nanosheets for ultrashort pulse generation in the near-infrared region*, Nanoscale **11**(13), 2019, pp. 6045–6051.

[16] SE YOON KIM, SANG BAE LEE, JOON CHUNG, *Highly stable optical add/drop multiplexer using polarization beam splitters and fiber Bragg gratings*, Photonics Technology Letters **9**(8), 1997, pp. 1119–1121.

[17] EISENMANN M., WEIDEL E., *Single-mode fused biconical coupler optimized for polarization beam splitting*, Journal of Lightwave Technology **9**(7), 1991, pp. 853–858.

[18] LUHUA XU, YUN WANG, AMAR KUMAR, *Polarization beam splitter based on MMI coupler with SWG birefringence engineering on SOI*, Photonics Technology Letters **30**(4), 2018, pp. 403–406.

[19] LIANGSHUN HAN, SONG LIANG, HONGLIANG ZHU, *A high extinction ratio polarization beam splitter with MMI couplers on InP substrate*, IEEE Photonics Technology Letters **27**(7), 2015, pp. 782–785.

[20] HONGNAN XU, DAOXIN DAI, LIU LIU, *Proposal for an ultra-broadband polarization beam splitter using anisotropy-engineered Mach-Zehnder interferometer on x-cut lithium-niobate-on-insulator*, Optics Express **28**(8), 2020, pp. 10899–10908.

[21] UEMATSU T., KITAYAMA T., ISHIZAKA Y., *Ultra-broadband silicon-wire polarization beam combiner/ splitter based on a wavelength insensitive coupler with a point-symmetrical configuration*, IEEE Photonics Journal **6**(1), 2014, article 4500108.

[22] XU Y., XIAO J., SUN X., *Compact polarization beam splitter for silicon-based slot waveguides using an asymmetrical multimode waveguide*, Journal of Lightwave Technology **32**(24), 2014, pp. 4282 –4288.

[23] SUN X., AITCHISON J.S., MOJAHEDI M., *Realization of an ultra-compact polarization beam splitter using asymmetric MMI based on silicon nitride/silicon-on-insulator platform*, Optics Express **25**(7), 2017, pp. 8296–8305.

[24] DAI D., WANG Z., PETERS J., BOWERS J.E., *Compact polarization beam splitter using an asymmetrical Mach–Zehnder interferometer based on silicon-on-insulator waveguides*, Photonics Technology Letters **24**(8), 2012, pp. 673–675.

[25] DAIGAO CHEN, XI XIAO, LEI WANG, *Broadband, fabrication-tolerant polarization beam splitters based on a tapered directional ccoupler*, Photonics Technology Letters **28**(9), 2016, pp. 2074–2077.

[26] CHAO-YI TAI, SHENG HSIUNG CHANG, TSENCHIEH CHIU, *Design and analysis of an ultra-compact and ultra-wideband polarization beam splitter based on coupled plasmonic waveguide arrays*, Photonics Technology Letters **19**(9), 2007, pp. 1448–1450.

[27] TIANYE HUANG, YUAN XIE, YIHENG WU, *Compact polarization beam splitter assisted by subwavelength grating in triple-waveguide directional coupler*, Applied Optics **58**(9), 2019, pp. 2264–2268.

[28] ZHANQIANG HUI, JIA-MIN GONG, MENG LIANG, *Demonstration of all-optical RZ-to-NRZ format conversion based on self-phase modulation in a dispersion flattened highly nonlinear photonic crystal fiber*, Optics & Laser Technology **54**(12), 2013, pp. 7–14.

[29] FLOROUS N., SAITOH K., KOSHIBA M., *A novel approach for designing photonic crystal fiber splitters with polarization in dependent propagation characteristics*, Optics Express **13**(19), 2005, pp. 7365 –7373.

[30] WENLIANG LU, SHUQIN LOU, XIN WANG, *Ultrabroadband polarization splitter based on a modified three-core photonic crystal fiber*, Applied Optics **52**(35), 2013, pp. 8494–8500.

[31] LINGHONG JIANG, YI ZHENG, LANTIAN HOU, *An ultrabraoadband polarization splitter based on square-lattice dual-core photonic crystal fiber with a gold wire*, Optics Communications **351**, 2015, pp. 50–56.

[32] WANG J., PEI L., WENG S., *Ultrashort polarization beam splitter based on liquid-filled dual-core photonic crystal fiber*, Applied Optics **57**(14), 2018, pp. 3847–3852.

[33] TONGTONG ZHAO, HAOQIANG JIA, ZHENGGANG LIAN, *Ultra-broadband dual hollow-core anti-resonant fiber polarization splitter*, Optical Fiber Technology **53**, 2019, article 102005.

[34] MASHANOVICH G.Z., MITCHELL C.J., SOLER PENADES J., *Germanium mid-Infrared photonic devices*, Journal of Lightwave Technology **35**(4), 2017, pp. 624–630.

[35] TING HU, BOWEI DONG, XIANSHU LUO, *Silicon photonic platforms for mid-infrared applications*, Photonics Research **5**(5), 2017, pp. 417–430.

[36] YUWEI QU, JINHUI YUAN, XIAN ZHOU, *et al.*, *Surface plasmon resonance-based silicon dual-core photonic crystal fiber polarization beam splitter at the mid-infrared spectral region*, Journal of the Optical Society of America B **37**(8), 2020, pp. 2221–2230.

[37] BOHAO ZHANG, WEIWEI CHEN, PENGJUN WANG, *Particle swarm optimized polarization beam splitter using metasurface-assisted silicon nitride Y-junction for mid-infrared wavelengths*, Optics Communications **451**, 2019, pp. 186–191

[38] KATO K., UMEMURA N., *Sellmeier equations for GaS and GaSe and their applications to the nonlinear optics in GaS_xSe_{1-x}*, Optics Letters **36**(5), 2011, p. 746.

[39] Bing Sun, Ming-Yang Chen, Jun Zhou, *Surface plasmon induced polarization splitting based on dual-core photonic crystal fiber with metal wire*, Plasmonics **8**, 2013, pp. 1253–1258.

[40] Haiming Jiang, Erlei Wang, Jing Zhang, *Polarization splitter based on dual-core photonic crystal fiber*, Optics Express **22**(25), 2014, pp. 30461–30466.

[41] Chen H.L., Li S.G., Fan Z.K.. *A novel polarization splitter based on dual-core photonic crystal fiber with a liquid crystal modulation core*, IEEE Photonics Journal **6**(4), 2014, article 2201109.

[42] Tongtong Zhao, Shuqin Lou, Xin Wang, *Ultrabroadband polarization splitter based on three-core photonic crystal fiber with a modulation core*, Applied Optics **55**(23), 2016, pp. 6428–6434.